Excited-State Hydroxide Ion Release From a Series of Acridinol Photobases

Yun Xie,[§,†] Stefan Ilic,[†] Sanja Skaro,[‡] Veselin Maslak,[‡] and Ksenija D. Glusac*,[†] [ID]

[†]Department of Chemistry, Center for Photochemical Sciences, Bowling Green State University, Bowling Green, Ohio 43403, United States

[‡]Faculty of Chemistry, University of Belgrade, Studentski Trg 12-16, Belgrade 11000, Serbia

ABSTRACT: The excited-state heterolysis of acridinol-based derivatives leads to the release of the OH^- ion and the formation of the corresponding acridinium cations. To evaluate the parameters that control the reaction barriers, the kinetics of excited-state OH^- release from a series of acridinol photobases were studied using transient absorption spectroscopy. The rate constants were obtained in three solvents (methanol, butanol, and isobutanol), and the data were modeled using Marcus theory. The intrinsic reorganization energies obtained from these fits were found to correlate well with the solvent reorganization energies calculated using dielectric continuum model, suggesting that the excited-state OH^- release occurs along the solvent reaction coordinate. Furthermore, the ability of acridinol photobases to photoinitiate chemical reactions was demonstrated using the Michael reaction between dimethylmalonate and nitrostyrene.
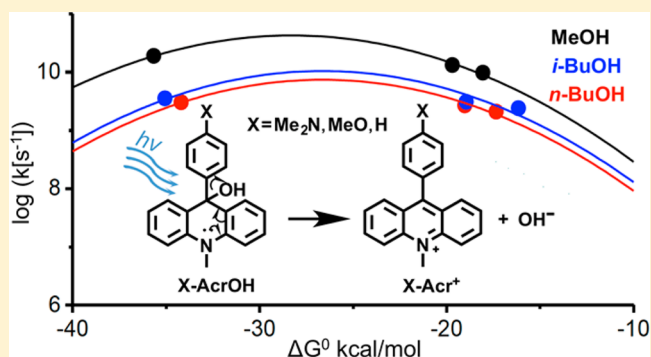
INTRODUCTION

Photoacids are a group of molecules, usually containing the aromatic alcohol motif, whose acidity significantly increases upon electronic excitation (up to 32 pK_a units).[1−3] The excitation of photoacids in the presence of appropriate base acceptors enables mechanistic studies of fast proton transfer (PT) reactions in solution using time-resolved laser techniques.[4−9] These experimental results provided a valuable platform to test and improve current theoretical models for PT. For example, Nibbering discovered the transient signature of the solvated proton in the mid-IR range during the PT between the pyranine photoacid and the acetate base, which offered evidence of a solvent-mediated PT.[7] Such solvent-mediated mechanism is not modeled in the traditional Eigen−Weller theory for PT, which prompted Siwick and Bakker to develop an improved model for PT that included a distribution of reactive acid−base species separated by a varying number of solvent molecules.[8] In addition to these basic studies of PT mechanism, the photoacids have also been applied to (i) generate and characterize short-lived intermediates, such as H_2CO_3;[10] (ii) probe the microenvironment of the biological systems (protein pockets and cells)[11−17] and other confined media (reverse micelles, cyclodextrins and nafion membranes);[18−20] (iii) study the protein folding kinetics using the pH jump technique.[21,22]

In analogy to the photoacids described above, the photobases are defined here as compounds that release hydroxide ion (OH⁻) upon excitation. Several types of photobases were identified in the 1980s and were composed of triarylmethanol,

xanthenol, fluorenol, and other molecular frameworks.[23,24] These early studies treated photobases as suitable sources of short-lived carbocations, whose reactivity with various nucleophiles was studied using time-resolved nanosecond laser spectroscopy.[25,26] More recently, the pseudobase derivatives of aryltropylium and acridinium ions have been investigated as a new class of photoswitches.[27−29] The kinetics of OH⁻ release were not addressed in these studies, likely due to the insufficient time resolution of the nanosecond transient absorption instrument used. Nowadays, the availability of ultrafast lasers allows chemists to capture the kinetics of OH⁻ release and investigate the mechanism of OH⁻ transport in various media, which will likely contribute to our understanding of OH⁻ solvation and diffusion. For example, recent findings have challenged the traditional view of OH⁻ solvation as $[OH(H_2O)_3]^-$ species, "mirror image" of proton solvation, and proposed a "hypercoordinated" configuration $[OH(H_2O)_4]^-$, which seems to agree with the experimental evidence.[30,31] With the unique light-triggered OH⁻ release, photobases will likely serve as an excellent probe for time-resolved studies of OH⁻ solvation. Furthermore, photobases have already been utilized to achieve spatiotemporal control in biologically relevant systems, to trigger DNA/RNA conformational changes and drug delivery.[32−34]

We previously studied the kinetics of OH⁻ release from an acridinol photobase using femtosecond pump−probe spectroscopy[35] and found that the heterolysis is fast (108 ps lifetime) in protic solvents (such as methanol), while no heterolysis occurs in aprotic solvent (such as acetonitrile). This solvent-dependent OH⁻ release is quite similar to the previous studies of excited-state PT[3] and is likely due to increased reactivity of the hydrogen-bonded complex between the photoacid or the photobase with the accepting solvent molecules. To gain a more quantitative comparison of the kinetics of H⁺/OH⁻ release, the intrinsic barrier for OH⁻ release from a xanthenol photobase was evaluated in a series of solvent mixtures.[36] Using the Marcus model, the intrinsic barrier was found to be $\Delta G_0^{\neq} \approx$ 10 kcal/mol, which is significantly higher than the barriers found previously for the PT ($\Delta G_0^{\neq} \approx$ 1−2 kcal/mol).[3,37] Such differences in the photoreactivity of photoacids and photobases could be due to differences in solvation of released ions. Alternatively, the lower reactivity of OH⁻ release could be due to high reorganization energy of the cation formed or due to less efficient OH⁻ release relative to H⁺.[36]

In this study, the role of the solvent reorganization on rates of excited-state OH⁻ release was evaluated using a series of acridinol photobases (Scheme 1). Specifically, the thermody-

Scheme 1. Photochemical OH⁻ Release from Model 9-Substituted Acridinols

X=Me₂N, MeO, H, CF₃, CN
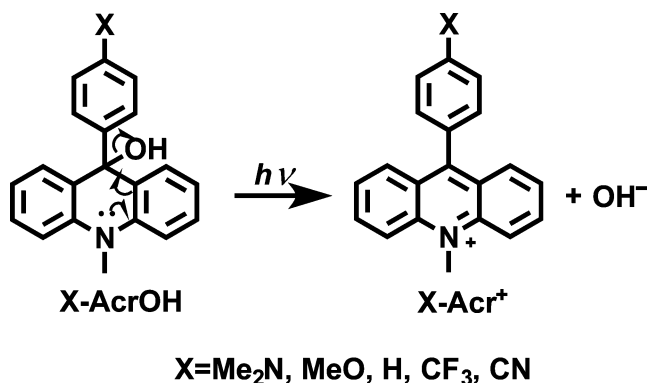
namics (ΔG) and kinetics (k) of the OH⁻ release were studied using steady-state and time-resolved UV/vis absorption spectroscopy. The experimental values were modeled using Marcus theory to evaluate the intrinsic barrier $\Delta G_0^{\neq}$ for the OH⁻ release. The intrinsic reorganization energies obtained from the Marcus fits were found to correlate very well with the solvent reorganization energies predicted by a dielectric continuum model. These results indicate that the OH⁻ release occurs along the solvent reaction coordinate and that the barrier height is controlled by the solvent response to the formed charges.

This manuscript also reports that the acridinol photobases can be utilized to drive chemical reactions. Previous approaches to photobase-driven reactions have mostly relied on bases protected with photolabile precursors.[38−40] While these methods provide efficient base generation, the process is irreversible. More recently, the reversibility was achieved using cis−trans photoisomerization as a way to control the basicity of the photoactive molecule.[41,42] Here, we show that the irradiation of acridinol photobase can be utilized to drive a Michael addition reaction. In specifics, the reaction between dimethylmalonate and nitrostyrene was triggered using AcrOMe photobase, which releases the methoxide ion upon

excitation. The methoxide ion acts as a base that deprotonates dimethylmalonate and initiates the addition to nitrostyrene. The results of this study show that acridinol photobases can promote the base-catalyzed reactions, which is expected to be useful in applications that require spatial or temporal control of the chemical reactivity.

EXPERIMENTAL SECTION

Syntheses. All chemicals were purchased from commercial suppliers and used without further purification. ¹H and ¹³C NMR spectra were recorded on a Bruker Avance III 500 MHz system. Electron impact ionization (EI) and matrix-assisted laser desorption ionization (MALDI) mass spectra were measured on a Shimadzu QP5050A and a Bruker Daltonics Omniflex mass spectrometer. 10-Methyl-9-phenylacridinium perchlorate (Acr⁺) was purchased from TCI America. Aryl bromides (4-bromoanisole, 4-bromobenzonitrile, and 4-bromo-benzotrifluoride) were purchased from Sigma. AcrOMe was synthesized according to already reported procedure.[35]

10-Methyl-9-phenyl-9,10-dihydroacridin-9-ol (AcrOH). AcrOH was synthesized according to the literature.[35] A 1 M solution of NaHCO₃ (100 mL) was added to 10-methyl-9-phenylacridinium perchlorate (Acr⁺, 225 mg, 0.6 mmol). Acetonitrile (∼25 mL) was added to dissolve Acr⁺ completely, and the pH was then increased to 13 by addition of 30% aqueous NaOH. Conversion was monitored using UV/vis by observing the disappearance of the absorption at 427 nm. When all Acr⁺ converted to AcrOH, the reaction mixture was stirred for 15 min in the dark. Acetonitrile was removed in vacuo, and water solution was extracted with dichloromethane (3 × 100 mL). Organic layers were combined and dried over anhydrous calcium chloride, and solvent was evaporated. Cyclohexane was added to the residue causing the precipitation of unreacted Acr⁺. Filtrate was collected and evaporated to give 95 mg of pure AcrOH (54%). MS-MALDI: m/z 287 [M⁺ for C₂₀H₁₇NO], ¹H NMR (CD₃CN, 500 MHz): δ 7.58 (d, 2H, J = 7.7 Hz), 7.35−7.31 (m, 2H), 7.22 (d, 4H, J = 4.3 Hz), 7.16−7.14 (m, 1H), 7.12 (d, 2H, J = 8.2 Hz), 7.01 (t, 2H, J = 7.5 Hz), 4.21 (br s, 1H), 3.49 (s, 3H). ¹³C NMR (CD₃CN, 125 MHz): δ 148.4, 140.0, 129.6, 128.1, 127.8, 126.7, 126.6, 125.6, 120.3, 112.4, 72.4, 32.7.

9-(4-(Dimethylamino)phenyl)-10-methylacridin-10-ium perchlorate (Me₂N-Acr⁺). Me₂N-Acr⁺ was synthesized according to the literature under modified conditions.[43] Under nitrogen, 10-methyl-9(10H)-acridone (1 g, 4.8 mmol), N,N-dimethylaniline (1.36 mL, 10.7 mmol, 2.3 equiv), and phosphoryl chloride (2.43 mL, 26.1 mmol, 5.4 equiv) were mixed and left to stir for 2 h at 90 °C. Concentrated aqueous sodium hydroxide solution was added carefully to quench the reaction. The reaction mixture was then extracted with dichloromethane; the organic layers were combined and dried over anhydrous sodium sulfate, and the solvent was evaporated under reduced vacuum. The oily residue was dissolved in minimal volume of acetonitrile, and perchloric acid was added until a green-yellowish color. Protonated Me₂NH⁺-Acr⁺ dication was then extracted with dichloromethane, and solvent was evaporated. Upon addition of water to the green-yellow solid, color changed to deep blue-purple. Target compound was extracted with dichloromethane and dried over anhydrous sodium sulfate, and solvent was evaporated. The crude solid product was recrystallized from acetonitrile/ether mixture. Formed precipitate was filtered and washed with copious amount of ether to yield 1.78 g of deep blue-purple solid

(90%). ^{1}H NMR (CD$_3$CN, 500 MHz): δ 8.54 (d, 2H, J = 9.2 Hz), 8.35 (dd, 1H, J_1 = 6.8 Hz, J_2 = 1.5 Hz), 8.33 (dd, 1H, J_1 = 6.8 Hz, J_2 = 1.5 Hz), 8.24 (dd, 2H, J_1 = 6.8 Hz, J_2 = 0.8 Hz), 7.85 (dd, 1H, J_1 = 6.8 Hz, J_2 = 0.8 Hz), 7.84 (dd, 1H, J_1 = 6.8 Hz, J_2 = 0.8 Hz), 7.48−7.45 (m, 2H), 7.13 (d, 2H, J = 7.9 Hz), 4.75 (s, 3H), 3.16 (s, 6H). ^{13}C NMR (CD$_3$CN, 125 MHz): δ 162.9, 151.9, 141.7, 138.6, 132.7, 131.0, 127.2, 126.1, 119.6, 118.6, 111.7, 40.2, 39.0.

9-(4-(Dimethylamino)phenyl)-10-methyl-4a,9,9a,10-tetra-hydroacridin-9-ol (Me$_2$N-AcrOH). Me$_2$N-Acr$^+$ (200 mg, 0.5 mmol) was dissolved in 10 mL of acetonitrile, and pH was increased to 13 by addition of 5 M aqueous NaOH solution. The resulting solution was stirred for 2 h and then extracted with dichloromethane. Organic layers were combined and dried over anhydrous sodium sulfate, and solvent was evaporated. Crude product was dissolved in hexane/benzene mixture (2:1) to precipitate the remaining starting material. Filtrate was collected and evaporated to give 85 mg of pure product (60%). MS-EI: m/z 312 [M$^+$ calculated for C$_{21}$H$_{16}$N$_2$O], ^{1}H NMR (CD$_3$CN, 500 MHz): δ 7.65 (dd, 2H, J_1 = 7.7 Hz, J_2 = 1.5 Hz), 7.34−7.31 (m, 2H), 7.10 (d, 2H, J = 8.3 Hz), 7.03 (td, 2H, J_1 = 7.7 Hz, J_2 = 1.1 Hz), 6.98−6.94 (m, 2H), 4.02 (br s, 1H), 3.46 (s, 3H), 2.84 (s, 6H). ^{13}C NMR (CDCl$_3$, 125 MHz): δ 162.8, 151.9, 141.6, 138.6, 132.7, 131.0, 127.2, 126.1, 119.6, 118.6, 113.3, 111.7, 77.2, 40.2, 39.0.

MeO-AcrOH, CN-AcrOH, and CF$_3$-AcrOH. These were synthesized according to the following procedure: To a solution of corresponding aryl bromide (2 mmol) in dry tetrahydrofuran (THF; 6 mL), 2.5 M hexane solution of *n*-butyllithium (0.96 mL, 2.4 mmol) was added dropwise at −78 °C under argon and stirred for 30 min. A suspension of 10-methyl-9(10H)-acridone (0.33 g, 1.6 mmol) in dry THF (14 mL) was then added, and the resulting solution was stirred for 12 h at room temperature. The reaction was quenched by addition of 20 mL of saturated aqueous ammonium chloride solution and extracted with dichloromethane (3 × 10 mL). Organic fractions were combined and dried over anhydrous magnesium sulfate, and solvent was evaporated. Crude product was dissolved in hexane/benzene mixture (2:1) causing the precipitation of the remaining starting material. The filtrate containing desired product was collected, and solvent was removed in vacuo to give desired acridinol.

9-(4-Methoxyphenyl)-10-methyl-9,10-dihydroacridin-9-ol (MeO-AcrOH). Using the procedure described above, 0.25 g of pure product (49%) was obtained. MS-EI: m/z 317 [M$^+$ calculated for C$_{21}$H$_{19}$NO$_2$], ^{1}H NMR (CD$_3$CN, 500 MHz): δ 7.62 (dd, 2H, J_1 = 7.7 Hz, J_2 = 1.5 Hz), 7.34 (dd, 1H, J_1 = 7.0 Hz, J_2 = 1.4 Hz), 7.33 (dd, 1H, J_1 = 7.0 Hz, J_2 = 1.4 Hz), 7.12 (d, 2H, J = 7.7 Hz), 7.10−7.07 (m, 2H), 7.03 (td, 2H, J_1 = 7.7 Hz, J_2 = 1.1 Hz), 6.77−6.74 (m, 2H), 4.11 (s, 1H), 3.72 (s, 3H), 3.48 (s, 3H). ^{13}C NMR (CD$_3$CN, 125 MHz): δ 158.3, 140.5, 140.1, 129.8, 128.0, 126.9, 126.4, 120.2, 113.0, 112.3, 72.0, 54.8, 32.9.

4-(9-Hydroxy-10-methyl-9,10-dihydroacridin-9-yl)-benzonitrile (CN-AcrOH). Using the given procedure, 0.31 g of pure product (48%) was obtained. MS-EI: m/z 312 [M$^+$ calculated for C$_{21}$H$_{16}$N$_2$O], ^{1}H NMR (CD$_3$CN, 500 MHz): δ 7.56−7.53 (m, 2H), 7.51 (dd, 2H, J_1 = 7.7 Hz, J_2 = 1.4 Hz), 7.39 (d, 2H, J = 8.3 Hz), 7.35−7.30 (m, 2H), 7.12 (d, 2H, J = 8.3 Hz), 6.98 (t, 2H, J = 7.5 Hz), 4.49 (s, 1H), 3.48 (s, 3H). ^{13}C NMR (CD$_3$CN, 125 MHz): δ 154.5, 140.7, 132.8, 129.5, 127.6, 127.2, 121.4, 113.6, 110.9, 72.9, 33.9.

10-Methyl-9-(4-(trifluoromethyl)phenyl)-9,10-dihydroacri-din-9-ol (CF$_3$-AcrOH): Using the given procedure, 0.39 g of pure product (55%) was obtained. MS-EI: m/z 355 [M$^+$ calculated for C$_{21}$H$_{16}$NF$_3$], ^{1}H NMR (CD$_3$CN, 500 MHz): δ 7.57−7.53 (m, 4H), 7.45 (d, 2H, J = 8.6 Hz), 7.36 (ddd, 2H, J_1 = 8.7 Hz, J_2 = 7.2 Hz, J_3 = 1.6 Hz), 7.16 (d, 2H, J = 8.3 Hz), 7.02 (td, 2H, J_1 = 7.8 Hz, J_2 = 1.6 Hz), 4.40 (s, 1H), 3.52 (s, 3H). ^{13}C NMR (CD$_3$CN, 125 MHz): δ 153.7, 140.7, 129.6, 129.4, 128.9 (q, J_{CF} = 32 Hz), 127.7, 127.1, 125.7 (q, J_{CF} = 3.8 Hz), 121.2, 113.5, 73.0, 33.8.

Equilibrium Constant Determination. UV/vis absorption spectra were recorded on Varian Cary 50 Bio spectrometer in a 1 cm quartz cell from 200 to 800 nm. The sample concentration was controlled so that the absorption maximum was ~1. Fluorescence measurements were performed on a single photon counting spectro-fluorimeter from Edinburgh Analytical Instruments (FL/FS 920) in a 1 cm quartz cell. The excitation wavelengths and the emission spectral windows were chosen according to each sample. The concentration of the samples was diluted 100 times from absorption measurements. The ground-state pK_{OH} values were determined as described previously with a slight modification.[35] The equilibrium constant K_{OH} was determined by titrating the solutions of acridinium cations (X-Acr$^+$) with a solution of sodium hydroxide with known concentration (it was assumed that NaOH fully dissociates in the solvent), and the concentrations of X-Acr$^+$ and X-AcrOH were determined using UV/vis absorption spectroscopy. The K_{OH} was calculated from the solution in which 50% of Acr$^+$ is converted to AcrOH, as

$$K_{OH} = [OH^-] = c_{NaOH} - \frac{c_{X\text{-}Acr^+}}{2}$$

Femtosecond Transient Absorption Experiments. The 800 nm laser pulses were produced at a 1 kHz repetition rate by a mode-locked Ti:sapphire laser and regenerative amplifier (Hurricane, Spectra-Physics). The output from the Hurricane was split into pump (85%) and probe (10%) beams. The pump beam was sent into an optical parametric amplifier (OPA-400, Spectra Physics) to obtain the desired excitation wavelength. The energy of the pump beam was <300 nJ/pulse. The probe beam was focused into a two-dimensional translated 4 mm CaF$_2$ crystal for white light generation between 350 and 800 nm. The flow cell (Starna Cell Inc. 45-Q-2, 0.9 mL volume with 2 mm path length), pumped by a Variable Flow Mini-Pump (Control Company), was used to prevent photodegradation of the sample. After it passed through the cell at the magic-angle geometry, the continuum was coupled into an optical fiber and input into a CCD spectrograph (Ocean Optics, S2000). The data acquisition was achieved using in-house LabVIEW (National Instruments) software routines. The group velocity dispersion of the probing pulse was determined using nonresonant optical Kerr effect (OKE) measurements. Sample solutions were prepared at a concentration needed to have absorbance of 1.0 at the excitation wavelength.

Photo-Michael Addition. The model Michael addition was performed by preparing a solution of 10.5 mg of *trans-β*-nitrostyrene (0.0706 mmol, 1 equiv), 8.1 μL of dimethylmal-onate (0.0706 mmol, 1 equiv), and 21.3 mg of AcrOMe (0.0706 mmol, 1 equiv) in 0.5 mL of methanol. The protocol involved either thermal or photochemical treatment. In the thermal treatment, the reaction mixture was stirred for 24 h at 65 °C. In the photochemical treatment, the reaction mixture was irradiated (125 W medium pressure mercury lamp) for 3

min and then stirred for 24 h at 65 °C. After each treatment, the reaction was quenched by addition of water, and the reaction mixture was extracted with dichloromethane. Organic layers were combined and dried over anhydrous sodium sulfate, and the solvent was evaporated. Oily crude product was purified with dry-flash chromatography (hexane/ethyl acetate = 8/2) to yield the oily product (thermal treatment gave 8.3 mg of the product or 38%, while the photochemical treatment gave 13 mg of the product or 60%). ^{1}H NMR (CDCl$_3$, 500 MHz): δ 7.34−7.28 (m, 3H), 7.24−7.22 (m, 2H), 4.95−4.86 (m, 2H), 4.24 (td, 1H J_1 = 9.0 Hz, J_2 = 5.1 Hz), 3.87 (d, 1H, J = 9.0 Hz), 3.76 (s, 3H), 3.56 (s, 3H). ^{13}C NMR (CDCl$_3$, 125 MHz): δ 168.0, 167.5, 136.4, 129.3, 128.6, 128.1, 77.6, 55.0, 53.2, 53.0, 43.2.

RESULTS AND DISCUSSION

Model compounds: The driving force for the excited-state OH$^-$ transfer was tuned by preparing a series of model acridinol compounds with varying substituents on the phenyl ring (Scheme 1). These acridinol derivatives were readily synthesized using a reaction between *N*-methyl-acridone and the corresponding aryl lithium reagent, as described in the Experimental Section. The absorption and emission spectra of the model acridinol photobases X-AcrOH and their corresponding acridinium salts X-Acr$^+$ are shown in Figure 1. In
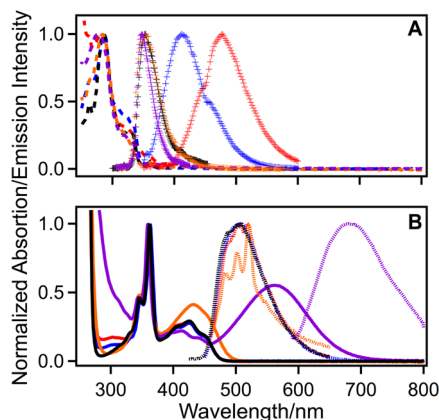

Figure 1. Absorption and emission spectra of (A) X-AcrOH and (B) X-Acr$^+$. All of the spectra were collected in acetonitrile at room temperature, except for Me$_2$N-Acr$^+$, whose emission spectrum was collected in 2-methyltetrahydrofuran at 77 K. AcrOH/Acr$^+$ (black), Me$_2$N-AcrOH/Me$_2$N-Acr$^+$ (purple), MeO-AcrOH/MeO-Acr$^+$ (orange), CF$_3$-AcrOH/CF$_3$-Acr$^+$ (blue), CN-AcrOH/CN-Acr$^+$ (red); X-AcrOH absorption (dash line), X-AcrOH emission (+ marker), X-Acr$^+$ absorption (solid line), X-Acr$^+$ emission (dotted line).

general, the absorption/emission maxima of all acridinol X-AcrOH derivatives appear at shorter wavelengths than the bands of the corresponding X-Acr$^+$ cations, which is consistent with the increased conjugation of the X-Acr$^+$ cations.

The red shifts in the absorption/emission bands were observed for the model compounds that can form charge-transfer excited states. For example, the emission bands of X-AcrOH derivatives with electron-withdrawing groups (478 nm for CN-AcrOH and 412 nm for CF$_3$-AcrOH) appear at higher wavelengths than the emission bands of other acridinols (~350 nm), which is likely due to the formation of charge-transfer excited state, in which the electron density migrates from the acridinol moiety to the substituted phenyl ring. Similarly, the

emission band of Me$_2$N-Acr$^+$ (680 nm) is red-shifted relative to emission bands of other acridinium cations (~510 nm), likely due to the formation of a charge-transfer state in which the electron density moves from the substituted phenyl ring to the acridinium moiety. Similar charge-transfer states were reported in other acridinium salts.[44]

THERMODYNAMICS

The thermodynamic driving force for the excited-state OH$^-$ release from model acridinol derivatives was evaluated in four different solvents (water, methanol, butanol, and isobutanol). First, the ground-state pK_{OH} and ΔG_{OH} values for the reaction

$$\text{X-AcrOH} \rightleftharpoons \text{X-Acr}^+ + \text{OH}^- \quad K_{OH} = \frac{[\text{X-Acr}^+][\text{OH}^-]}{[\text{X-AcrOH}]} \tag{1}$$
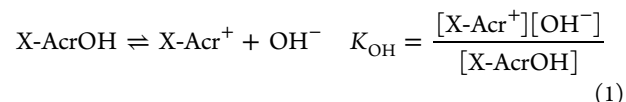
were obtained using pH-dependent UV/vis absorption spectroscopy. The results indicate that the OH$^-$ release from acridinol models in their ground state is thermodynamically unfavorable in all solvents (Table 1). The thermodynamic

Table 1. Ground-State pK_{OH} and ΔG_{OH} Values for Model X-AcrOH Acridinols in Different Solvents

	H$_2$O		MeOH		*n*-BuOH[a]		*i*-BuOH[a]	
X	pK_{OH}	ΔG_{OH}	pK_{OH}	ΔG_{OH}	pK_{OH}	ΔG_{OH}	pK_{OH}	ΔG_{OH}
Me$_2$N	2.3	3.2	4.0	5.5	5.1	7.0	4.4	6.1
MeO	2.7	3.7	4.5	6.1	4.9	6.8	5.0	6.8
H	2.8	3.9	4.7	6.4	5.2	7.2	6.1	8.3
CF$_3$	3.2	4.4	5.6	7.7				
CN	3.3	4.5	5.8	8.0				

[a]The calculations assume that NaOH fully dissociates in *n*-BuOH and *i*-BuOH.

parameters for CF$_3$-AcrOH and CN-AcrOH in *n*-BuOH and *i*-BuOH were not obtained, because the excited-state OH$^-$ release was not observed for these X-AcrOH/solvent systems. Across the acridinol series, the driving force increases with the electron-donating character of the substituent (e.g., the lowest ΔG value was obtained for Me$_2$N-AcrOH). This result is consistent with the fact that electron-donating groups stabilize the X-Acr$^+$ cations formed upon OH$^-$ release by positive charge delocalization. Similarly, previous studies have shown that the driving force for OH$^-$ release in other pseudobases correlates well with factors that tend to stabilize the corresponding cations.[45−47] For example, the driving force for OH$^-$ release from xanthenol (XanOH) in water is ΔG = 18.8 kcal/mol,[36] which is significantly higher than for acridinol AcrOH (ΔG = 3.9 kcal/mol), reflecting the higher aromatic character of acridinium cation Acr$^+$ relative to Xan$^+$. The solvent effects on the driving force is as expected: the high-polarity solvents (water) are better at stabilizing the ions formed upon heterolysis, which lowers the ΔG values for OH$^-$ release. Similar solvent polarity effects were observed in the photo-acids.[48]

The ground-state pK_a values were then used to derive the excited-state thermodynamics using the Förster cycle,[35] as follows:

$$\Delta G_{OH}^* = h\nu_{\text{X-AcrOH}} - \Delta G_{OH} - h\nu_{\text{X-Acr}^+} \tag{2}$$

For this purpose, the frequencies for 0−0 transitions of X-AcrOH and X-Acr$^+$ were derived from the emission spectra of

Table 2. Excited-State pK^*_{OH} and ΔG^*_{OH} Values for Model X-AcrOH Acridinols in Different Solvents

	H$_2$O		MeOH		n-BuOH		i-BuOH	
X	pK^*_{OH}	ΔG^*_{OH}	pK^*_{OH}	ΔG^*_{OH}	pK^*_{OH}	ΔG^*_{OH}	pK^*_{OH}	ΔG^*_{OH}
Me$_2$N	−27.2	−37.3	−25.5	−35.7	−25.1	−34.2	−25.8	−35.1
MeO	−16.1	−22.1	−14.4	−19.7	−13.9	−19.0	−13.8	−19.0
H	−15.0	−20.6	−13.2	−18.1	−12.7	−17.4	−11.8	−16.2
CF$_3$	−6.4	−8.8	−3.9	−6.0				
CN	0.7	1.0	3.3	4.4				

the model compounds (Figure 1). The resulting ΔG_{OH}* values (Table 2) show that the driving force for OH$^-$ release considerably increases upon excitation. For example, the driving force for Me$_2$N-AcrOH in methanol changes from 5.5 kcal/mol in the ground state to −35.7 kcal/mol in the excited state. In other acridinols, similar but less drastic changes in ΔG values occur, and the excited-state OH$^-$ release is thermodynamically favored in all compounds except for CN-AcrOH.

The experimental pK_{OH} and pK^*_{OH} values correlate linearly with the Hammett σ coefficients[49] for the X-substituents (Figure 2), demonstrating that the simple free-energy relation-
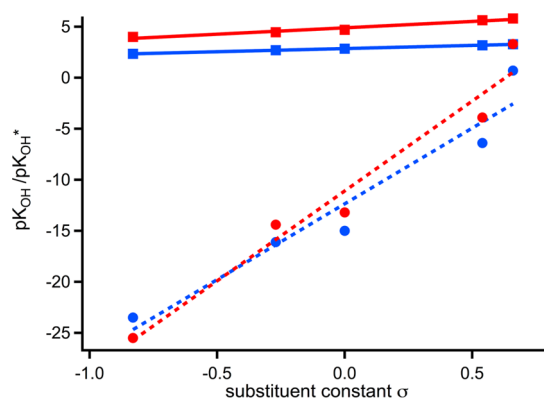

Figure 2. Hammet plots for ground (■ and solid lines) and excited-state (● and dashed lines) OH$^-$ release from X-AcrOH in water (blue) and methanol (red). The slopes are as follows: for ground states $\rho = 0.6$ in water and 1.2 in methanol; for excited-states $\rho^* = 14.8$ in water and 17.6 in methanol.

ship concept can be used efficiently to predict the driving force for the OH$^-$ release. Similar linear relationship with a slope of opposite sign was observed for the photoacids,[34] indicating that the driving force for H$^+$ or OH$^-$ release is controlled by stabilization of charges formed upon the ion release (RO$^-$ for photoacids and R$^+$ for photobases). Interestingly, the slope ρ is significantly steeper for the excited-state pK^*_{OH} values ($\rho^* = 14.8$ in water) than for the ground-state pK_{OH} values ($\rho = 0.6$ in water). Thus, the electron-donating substituents in the X-position appear to stabilize more efficiently the positive charge of X-Acr$^+$ in its S$_1$ state than in the S$_0$ state. Similar effects were observed in naphthol-based photoacids, where the substituent effects were found to correlate with the calculated charge densities of relevant atoms in their ground and excited states.[3] It is likely that a similar effect holds for X-AcrOH photobases.

■ KINETICS

The rates of OH$^-$ release from model acridinols were determined using pump−probe spectroscopy. The spectral changes in the visible range were consistent with the photochemical heterolysis of the C−O bond (Figure 3). For
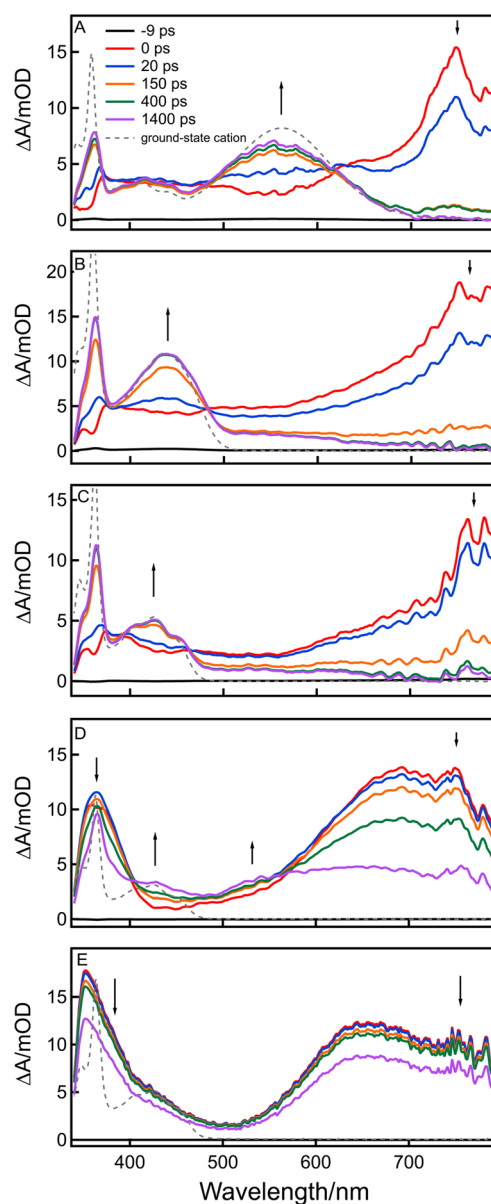

Figure 3. Femtosecond transient absorption spectra of X-AcrOH in MeOH at several time delays after the 310 nm excitation pulse: (A) Me$_2$N-AcrOH; (B) MeO-AcrOH; (C) AcrOH; (D) CF$_3$-AcrOH; (E) CN-AcrOH. The dashed lines represent the ground-state absorption spectra for the corresponding X-Acr$^+$ cations.

example, the transient absorption spectrum of the methanol solution of Me$_2$N-AcrOH at early times (red trace, Figure 3A) was assigned to its S$_1$ state and exhibited broad features throughout the visible range with $\lambda_{max} = 748$ nm. The S$_1$ signal decayed within few hundreds picoseconds and was accompanied by a concomitant growth of a new transient that

absorbed at λ_{max} = 553 nm. The absorption spectrum of this growing transient matched well to the spectrum of Me$_2$N-Acr$^+$ cation in the S$_0$ state (Figure 3A, dashed line), which is consistent with the excited-state OH$^-$ release from Me$_2$N-AcrOH. In a similar fashion, the conversion from excited MeO-AcrOH, AcrOH, and CF$_3$-AcrOH in methanol leads to the formation of the corresponding cations (Figure 3B–D). In the case of CN-AcrOH, the excited-state OH$^-$ release was not observed, which is consistent with the unfavorable thermodynamics (ΔG^* = +1.0 kcal/mol, Table 2) and shows that the rates of the OH$^-$ release correlate with the ΔG^* values calculated using simple Förster cycle.

Two similarities can be drawn between the photoheterolysis observed in photoacids[37,50] and the photobases studied here: (i) the rates of heterolysis correlate well with the driving force for the adiabatic process (ΔG^*), as discussed in the previous paragraph; (ii) the excited-state heterolysis occurs predominantly in protic solvents (such as alcohols). For example, MeO-AcrOH undergoes efficient excited-state OH$^-$ release in n-BuOH (Figure 4A), while S$_1$ → T$_1$ intersystem crossing
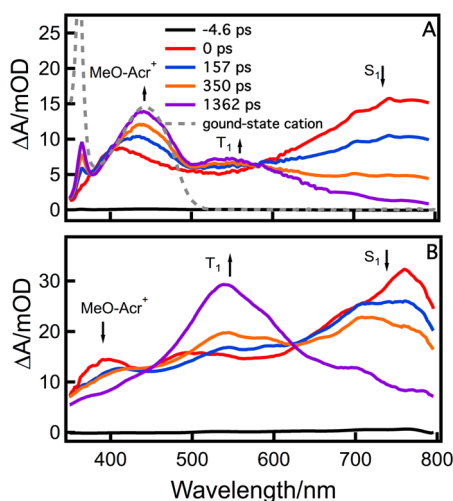

Figure 4. Femtosecond transient absorption data for MeO-AcrOH in (A) n-BuOH and (B) ACN. The samples were excited at 310 nm.

(ISC) occurs in acetonitrile (Figure 4B). Such dependence is suggestive of the important role that the solvent reorganization energy plays in the H$^+$ and OH$^-$ release from organic alcohols.[2,48] One notable difference exists between the excited-state behavior of photoacids and photobases: the PT generally occurs adiabatically, while the OH$^-$ transfer occurs nonadiabatically in most photobases. For example, on the one hand, the fluorescence spectra of photoacids in protic solvents generally contain a variable degree of the red-shifted emission due to the conjugate base formed upon the PT, confirming its adiabatic nature.[51] On the other hand, the transient absorption spectra of X-AcrOH derivatives (Figure 3 and ref 35) show that X-Acr$^+$ cations are formed in the ground state, suggesting a nonadiabatic process. To the best of our knowledge, only two previous reports showed adiabatic OH$^-$ release from a xanthenol photobase,[23,52] but even in this case the adiabatic process was a minor heterolysis channel, while most of the OH$^-$ release occurred nonadiabatically.

The kinetics of S$_1$ states in all model X-AcrOH derivatives can be readily obtained by probing the red portion of the visible spectrum (for example λ = 750 nm, Figure 5). The observed
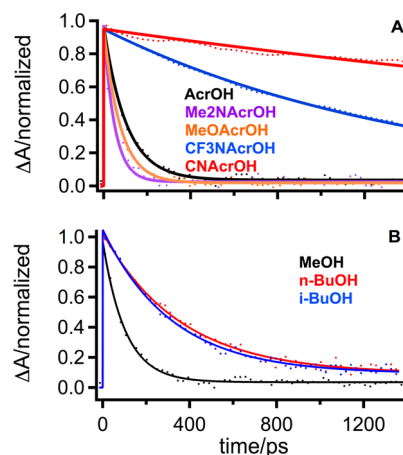

Figure 5. (A) Normalized transient absorption traces (λ_{probe} = 750 nm) for X-AcrOH solutions in MeOH (λ_{pump} = 310 nm). Lifetime: Me$_2$N-AcrOH 53 ps; MeO-AcrOH 76 ps; AcrOH 108 ps; CF$_3$-AcrOH 1.4 ns; CN-AcrOH 6.3 ns. (B) The kinetic trace for AcrOH (λ_{pump} = 310 nm; λ_{probe} = 750 nm) in MeOH (108 ps), n-BuOH (357 ps), and i-BuOH (319 ps).

rate of S$_1$ decay increases along X-AcrOH series (Figure 5A), with faster decay occurring for electron-donating groups (such as Me$_2$N-AcrOH). The result is consistent with the ΔG^* values listed in Table 2: the photoheterolysis rate increases as the process becomes more thermodynamically favorable. The solvent effects on the rate of OH$^-$ release are shown in Figure 5B: the faster heterolysis is observed in higher-polarity solvent (the solvent dielectric constants are as follows: ε_{MeOH} = 33.0, $\varepsilon_{n\text{-}BuOH}$ = 17.8, $\varepsilon_{i\text{-}BuOH}$ = 17.9[53]). The solvent effects are consistent with increased stability of product ions by polar solvents, and this stabilization is reflected in the thermodynamic driving forces (Table 2). The polarities of n-BuOH and i-BuOH are similar, but i-BuOH is bulkier. The observed rate does not change significantly in the two solvents, indicating that the solvent polarity plays the deciding role on the rate of OH$^-$ release.

In all model compounds, the 750 nm signal exhibited monoexponential decay with rate constants k_{exp} (Table 3). As the rate of OH$^-$ release slows across the X-AcrOH series, the process starts to compete with the S$_1$ → T$_1$ ISC. Our earlier work on AcrOH[35] showed that the excited-state OH$^-$ release occurs only in protic solvents (methanol), while ISC dominates the excited-state deactivation in aprotic solvents (acetonitrile). Similar behavior in aprotic solvents was observed for most X-AcrOH derivatives (data not shown), which allowed the determination of ISC rates for each acridinol (k_{ISC}). The competition between heterolysis and ISC can be visualized in the case of CF$_3$-AcrOH (Figure 3D). In addition to the growth of CF$_3$-Acr$^+$ absorption bands (λ_{ABS} = 425 nm), additional absorption appears in the 500−600 nm range and is assigned to the T$_1$ state of CF$_3$-AcrOH. Thus, the rates for OH$^-$ release were obtained as follows:

$$k_{OH} = k_{exp} - k_{ISC} \tag{3}$$

The resulting k_{OH} values are listed in Table 3. The use of eq 3 assumes that the rate of ISC does not change significantly when going from acetonitrile to the alcohols studied here. Such assumption likely introduced an error in the estimated k_{OH} values, since previous reports indicate that some compounds exhibit relatively strong solvent effects on their ISC rates.[54,55]

Table 3. Experimental Rate Constants (k_{exp}) for the Singlet Excited-State Decays of X-AcrOH Models and the Derived Rates for OH$^-$ Release (k_{OH}) Determined As Described in the Text

	MeOH		n-BuOH		i-BuOH	
X	$k_{exp}/1 \times 10^9$ s^{-1}	$k_{OH}/1 \times 10^9$ s^{-1}	$k_{exp}/1 \times 10^9$ s^{-1}	$k_{OH}/1 \times 10^9$ s^{-1}	$k_{exp}/1 \times 10^9$ s^{-1}	$k_{OH}/1 \times 10^9$ s^{-1}
Me$_2$N	0.2	0.2	3.7	3.0	4.3	3.6
MeO	0.1	0.1	3.4	2.4	3.8	2.9
H	9.3	9.3	3.1	2.4	3.1	2.4
CF3	70.9	53.3				
CN	15.9					

However, since the triplet excited-state absorption energy does not change significantly in different solvents (e.g., triplet excited state of MeO-AcrOH absorbs at 550 nm in both ACN and n-BuOH, Figure 4), it is likely that the above assumption is justified.

The obtained k_{OH} values were used to construct their dependence on the thermodynamic driving force (Figure 6).
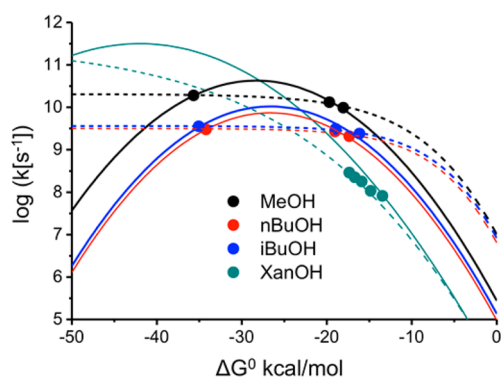
Figure 6. Dependence of k_{OH} values on thermodynamic driving forces for the excited-state OH$^-$ release from model X-AcrOH derivatives. The fits were obtained using either Marcus (solid lines) or BEBO (dashed lines) model. The results of a previous study involving a xanthenol (XanOH) photobase[36] in acetonitrile/water mixtures are included for comparison.

To model the rate constant dependence on the thermodynamic driving force, the well-known transition-state theory expression was used. It relates the rate constants with the corresponding energy barriers:

$$k = A \cdot e^{-\Delta G^{\neq}/R \cdot T} \quad (4)$$

where A is the pre-exponential factor and $\Delta G\ddagger$ is the Gibbs free energy for the transition state. Two theoretical models were then used to correlate the dependence of $\Delta G\ddagger$ on the thermodynamic driving force ΔG^0. One treatment utilized the Marcus model,[56−59] which has been successfully applied to group transfers in which reaction rate is controlled by the response of the solvent to the charge redistribution. In this case, the reaction proceeds along the solvent reaction coordinate, and the free energy correlation is

$$\Delta G^{\neq} = \left(1 + \frac{\Delta G^{\circ}}{4 \cdot \Delta G_0^{\neq}}\right)^2 \cdot G_0^{\neq} \quad (5)$$

where $\Delta G_0^{\neq}$ is the activation energy for the symmetric group transfer ($\Delta G^0 = 0$). The second treatment utilized the bond-energy bond-order (BEBO) theory,[60−62] which models reactions that occur in a strong coupling regime, where the bond stretching and compression define the reaction

coordinate. The BEBO model evaluates the energy of a reacting system at any point along the reaction coordinate using a linear combination of reactant and product energies, which are scaled by their bond order at a given point of the reaction coordinate. According to BEBO model, the free energy correlation is expressed as

$$\Delta G^{\neq} = \frac{\Delta G^{\circ}}{2} + \Delta G_0^{\neq} + \frac{\Delta G_0^{\neq}}{\ln 2} \cdot \ln\left(\cosh\left(\frac{\Delta G^{\circ} \cdot \ln 2}{2 \cdot \Delta G_0^{\neq}}\right)\right) \quad (6)$$

At lower driving forces, both Marcus and BEBO models predict similar rate dependence on the driving force, where the rate increases with increasing driving force. At large driving forces, however, the two models predict different behavior: while the Marcus model predicts a decrease in the rate at high driving forces (inverted region), the BEBO model predicts the rates to level off at high driving forces (Figure 6). In the case of OH$^-$ release from photobases, it is not known whether the rate-determining process involves predominantly the solvent reorganization or the reorganization of the molecular bonds; therefore, the data were evaluated using both models.

Unfortunately, the limited range and number of experimental data points precluded us from evaluating whether Marcus or BEBO theory is better at modeling the excited-state OH$^-$ release from our model compounds. However, it is interesting to note that the reorganization energies λ obtained using the Marcus model (Table 4) for AcrOH photobases in alcohol-

Table 4. Summary of the Parameters Obtained from Marcus and BEBO Analyses

|	Marcus				BEBO	
solvent	A	$\Delta G_0^{\neq}$ kcal/mol	λ^b kcal/mol	λ_s kcal/mol	A	$\Delta G_0^{\neq}$ kcal/mol
ACN/H$_2$O^a	11.5	10.8	43.2	29.1−30.5	11.5	10.2
MeOH	10.6	7.1	28.3	29.8	10.3	4.5
n-BuOH	9.9	6.7	26.6	25.2	9.5	3.7
i-BuOH	10.0	6.7	26.6	25.3	9.6	3.6

^{a}For XanOH photobase, taken from ref 36. $^b\lambda = 4\Delta G_0^{\neq}$.

based solvents match reasonably well with the expected solvent reorganization energies λ_s at the contact distance calculated using the dielectric continuum expression[63,64]

$$\lambda_s = \frac{e^2}{4\pi\varepsilon_0}\left(\frac{1}{2r_D} + \frac{1}{2r_A} - \frac{1}{r}\right)\left(\frac{1}{\varepsilon_{op}} - \frac{1}{\varepsilon_s}\right) \cdot N_A \quad (7)$$

where ε_{op} and ε_s are optical and static dielectric constants of the solvent, r_D and r_A are the donor and acceptor radii (we assumed that the radii are 3 Å each), and r is the distance between donor

Scheme 2. Model Photo-Michael Addition between Nitrostyrene and Dimethylmalonate Using a Light-Triggered Base AcrOMe
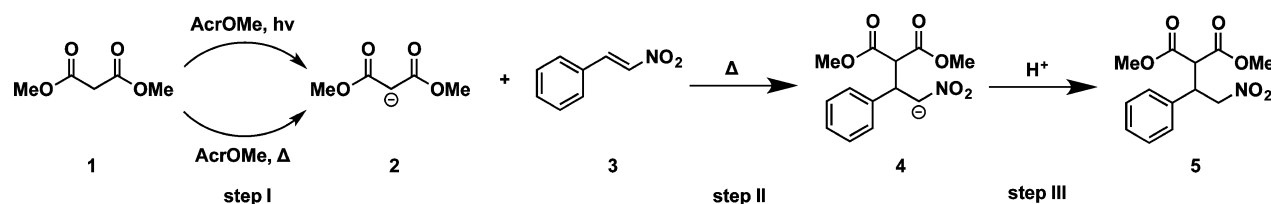
and acceptor. On the basis of these values, it appears that the excited-state OH⁻ release from model acridinol photobases occurs along the reaction coordinate involving solvent responses and can be predicted well using the Marcus model.

The above results obtained in alcohol solvents are in contrast with the results reported in our previous study involving xanthenol (XanOH) photobase in acetonitrile/water mixtures.[36] The Marcus fit from this study provided a value for reorganization energy of $\lambda = 43.2$ kcal/mol, which is significantly higher than the solvent reorganization energy of $\lambda_s = 29.1-30.5$ kcal/mol calculated using the dielectric continuum model for acetonitrile and water (Table 4). Since the structures of XanOH and AcrOH photobases are quite similar, the differences in reorganization energies are likely due to solvents used. The dielectric continuum model is known to fail in predicting the solvent reorganization energies in cases when there are specific reactant–solvent interactions.[65−67] When such noncontinuum factors are present, the experimentally observed rates are generally slower than those predicted by the continuum model, which is consistent with our results for XanOH in water/ACN mixtures.[36]

PHOTO-MICHAEL ADDITION

The utility of photobases to drive chemical reaction has been reported previously, namely, to drive Henry[41] and thiol-Michael additions.[68,69] In both of these examples, the photochemical event generates an amine, which serves as a base to drive the chemical reaction of interest. In a similar fashion, the acridine photobases could be utilized to drive photochemically the reactions that require either hydroxide ions or other anionic species (such as alkoxide ions). To investigate this possibility, AcrOMe derivative was used as a system that, upon excitation, releases methoxide (MeO⁻) ion. The photogenerated MeO⁻ ions were successfully utilized in a model Michael addition between dimethylmalonate 1 and nitrostyrene 3 (Scheme 2), in a reaction that involves three individual steps: (i) deprotonation of malonate 1 using the photogenerated MeO⁻ ions; (ii) nucleophilic attack of the enolate 2 to the electron-deficient C═C bond of nitrostyrene 3; (iii) protonation of the intermediate 4 to give the final product 5.

While Michael additions often require only catalytic amounts of the base, the model reaction presented in Scheme 2 requires stoichiometric amounts of the MeO⁻ ion. Experiments that utilized a lower number of MeO⁻ equivalents yielded less product, indicating that the turnover frequency (TOF) of the catalytic cycle is not sufficiently high to compete with other unwanted chemical reactions. The likely reason for low catalytic TOF is the low basicity of the intermediate 4, which prevents it from abstracting a proton from malonate 1 (a step that is needed to close the catalytic cycle): the acidity of compound 5 is expected to be similar to that of nitromethane ($pK_a = 10$),[70] while the acidity of malonate 1 is $pK_a = 13$.[71] However, this model reaction is expected to serve as a proof-of-principle study

for development of future reactions in which the pK_a values of relevant reactants are tailored toward catalysis.

When the reaction mixture containing AcrOMe was photoirradiated, the product yield was found to be 60%. The reaction mixture was heated to 65 °C, since the addition step II does not occur at room temperature. When the same reaction was performed in the absence of light, the product yield was only 38%, indicating that the AcrOMe performance can be significantly improved using photochemical methods. However, the results show that reaction occurs even in the absence of irradiation, possibly due to the thermal heterolysis of AcrOMe bond. This finding is consistent with the fact that the Gibbs free energy for AcrOMe heterolysis is expected to be $\Delta G_{OMe} \approx 6.4$ kcal/mol (similar to that of AcrOH, Table 1). At the reaction temperature of 65 °C, at least 1% of the AcrOMe is expected to thermally dissociate into Acr⁺ and MeO⁻ ions, which can drive the "dark" Michael addition. The contrast in the reaction yields between the dark and photochemical Michael reactions can likely be increased if the choice of reactants was made to perform the reaction at room temperature.

CONCLUSIONS

The excited-state OH⁻ transfer has been studied to a lesser degree relative to the corresponding PT reactions. This manuscript aims to bridge the gap by investigating the parameters that affect the kinetics of the OH⁻ release from model acridinol photobases. The thermodynamic driving force for the reaction was tuned using a series of acridinol derivatives with varying substituents on the phenyl ring, while the reaction rates were determined using time-resolved laser spectroscopy. The experimentally obtained rate constants and Gibbs free energies were fit using the Marcus model for group transfer reactions. The fitted data provided an intrinsic reorganization energy, which matches surprisingly well with the solvent reorganization energies calculated using a simple dielectric continuum model. The results of this study indicate that the solvent reorganization plays a major role in the kinetics of the excited-state OH⁻ release and can be efficiently modeled using the Marcus model. These results are in contrast to our previous study involving a xanthenol photobase in acetonitrile/water mixtures,[36] where the experimentally obtained reorganization energy was significantly higher than the solvent reorganization energy predicted by the dielectric continuum model. The observed discrepancy could be due to strong specific solvent–solute interactions present in aqueous environment.

This manuscript also evaluates the utilization of acidinol photobases in driving useful chemical reactions. Specifically, the Michael addition between dimethylmalonate and nitrostyrene was successfully performed using MeO⁻ base that was photochemically generated from the corresponding AcrOMe derivatives. While the reported reaction also occurred thermally (with a lower yield), the results indicate that the photo-Michael addition reported here can be further optimized and developed

into a useful photochemical tool for applications where spatial-temporal control is needed.

■ AUTHOR INFORMATION

Corresponding Author

*E-mail: kglusac@bgsu.edu.

ORCID ⓘ

Ksenija D. Glusac: 0000-0002-2734-057X

Present Address

§Department of Petroleum Engineering, University of Wyoming, Laramie, Wyoming 82071, United States.

Notes

The authors declare no competing financial interest.

■ REFERENCES

(1) Arnaut, L. G.; Formosinho, S. J. Excited-State Proton Transfer Reactions I. Fundamentals and Intermolecular Reactions. *J. Photochem. Photobiol., A* **1993**, *75* (1), 1–20.

(2) Tolbert, L. M.; Solntsev, K. M. Excited-State Proton Transfer: From Constrained Systems to "Super" Photoacids to Superfast Proton Transfer. *Acc. Chem. Res.* **2002**, *35* (1), 19–27.

(3) Agmon, N. Elementary Steps in Excited-State Proton Transfer. *J. Phys. Chem. A* **2005**, *109* (1), 13–35.

(4) Huppert, D.; Kolodney, E.; Gutman, M.; Nachliel, E. Effect of Water Activity on the Rate of Proton Dissociation. *J. Am. Chem. Soc.* **1982**, *104* (25), 6949–6953.

(5) Agmon, N.; Huppert, D.; Masad, A.; Pines, E. Excited-State Proton Transfer to Methanol-Water Mixtures. *J. Phys. Chem.* **1991**, *95* (25), 10407–10413.

(6) Rini, M.; Magnes, B.-Z.; Pines, E.; Nibbering, E. T. Real-Time Observation of Bimodal Proton Transfer in Acid-Base Pairs in Water. *Science* **2003**, *301* (5631), 349–352.

(7) Mohammed, O. F.; Pines, D.; Dreyer, J.; Pines, E.; Nibbering, E. T. Sequential Proton Transfer Through Water Bridges in Acid-Base Reactions. *Science* **2005**, *310* (5745), 83–86.

(8) Siwick, B. J.; Bakker, H. J. On the Role of Water in Intermolecular Proton-Transfer Reactions. *J. Am. Chem. Soc.* **2007**, *129* (44), 13412–13420.

(9) Liu, W.; Han, F.; Smith, C.; Fang, C. Ultrafast Conformational Dynamics of Pyranine during Excited State Proton Transfer in Aqueous Solution Revealed by Femtosecond Stimulated Raman Spectroscopy. *J. Phys. Chem. B* **2012**, *116* (35), 10535–10550.

(10) Adamczyk, K.; Prémont-Schwarz, M.; Pines, D.; Pines, E.; Nibbering, E. T. Real-Time Observation of Carbonic Acid Formation in Aqueous Solution. *Science* **2009**, *326* (5960), 1690–1694.

(11) Das, R.; Mitra, S.; Nath, D.; Mukherjee, S. Excited State Proton Transfer Reaction as a Probe for the Microenvironment of a Binding Site of Bovine Serum Albumin: Effect of Urea. *J. Phys. Chem.* **1996**, *100* (34), 14514–14519.

(12) Nachliel, E.; Pollak, N.; Huppert, D.; Gutman, M. Time-Resolved Study of the Inner Space of Lactose Permease. *Biophys. J.* **2001**, *80* (3), 1498–1506.

(13) Cohen, B.; Martin Álvarez, C.; Alarcos Carmona, N.; Organero, J. A.; Douhal, A. Proton-Transfer Reaction Dynamics within the Human Serum Albumin Protein. *J. Phys. Chem. B* **2011**, *115* (23), 7637–7647.

(14) Shvadchak, V. V.; Falomir-Lockhart, L. J.; Yushchenko, D. A.; Jovin, T. M. Specificity and Kinetics of α-Synuclein Binding to Model Membranes Determined with Fluorescent Excited State Intramolecular Proton Transfer (ESIPT) Probe. *J. Biol. Chem.* **2011**, *286* (15), 13023–13032.

(15) Chowdhury, R.; Saha, A.; Mandal, A. K.; Jana, B.; Ghosh, S.; Bhattacharyya, K. Excited State Proton Transfer in the Lysosome of Live Lung Cells: Normal and Cancer Cells. *J. Phys. Chem. B* **2015**, *119* (6), 2149–2156.

(16) van Thor, J. J. Photoreactions and Dynamics of the Green Fluorescent Protein. *Chem. Soc. Rev.* **2009**, *38* (10), 2935–2950.

(17) Chattoraj, M.; King, B. A.; Bublitz, G. U.; Boxer, S. G. Ultra-Fast Excited State Dynamics in Green Fluorescent Protein: Multiple States and Proton Transfer. *Proc. Natl. Acad. Sci. U. S. A.* **1996**, *93* (16), 8362–8367.

(18) Gepshtein, R.; Leiderman, P.; Huppert, D.; Project, E.; Nachliel, E.; Gutman, M. Proton Antenna Effect of the γ-Cyclodextrin Outer Surface, Measured by Excited State Proton Transfer. *J. Phys. Chem. B* **2006**, *110* (51), 26354–26364.

(19) Cohen, B.; Huppert, D.; Solntsev, K. M.; Tsfadia, Y.; Nachliel, E.; Gutman, M. Excited State Proton Transfer in Reverse Micelles. *J. Am. Chem. Soc.* **2002**, *124* (25), 7539–7547.

(20) Spry, D.; Goun, A.; Glusac, K.; Moilanen, D. E.; Fayer, M. Proton Transport and the Water Environment in Nafion Fuel Cell Membranes and AOT Reverse Micelles. *J. Am. Chem. Soc.* **2007**, *129* (26), 8122–8130.

(21) Abbruzzetti, S.; Viappiani, C.; Small, J. R.; Libertini, L. J.; Small, E. W. Kinetics of Histidine Deligation from the Heme in GuHCl-Unfolded Fe (III) Cytochrome C Studied by a Laser-Induced pH-Jump Technique. *J. Am. Chem. Soc.* **2001**, *123* (27), 6649–6653.

(22) Kohse, S.; Neubauer, A.; Pazidis, A.; Lochbrunner, S.; Kragl, U. Photoswitching of enzyme activity by laser-induced pH-jump. *J. Am. Chem. Soc.* **2013**, *135* (25), 9407–9411.

(23) Wan, P.; Yates, K.; Boyd, M. K. Adiabatic Photodehydroxylation of 9-Phenylxanthen-9-ol. Observation of Carbocation Fluorescence in Neutral Aqueous Solution. *J. Org. Chem.* **1985**, *50* (16), 2881–2886.

(24) Wan, P.; Krogh, E. Contrasting Photosolvolytic Reactivities of 9-Fluorenol vs. 5-Suberenol Derivatives. Enhanced Rate of Formation of Cyclically Conjugated 4π Carbocations in the Excited State. *J. Am. Chem. Soc.* **1989**, *111* (13), 4887–4895.

(25) Wan, P.; Shukla, D. Utility of Acid-Base Behavior of Excited States of Organic Molecules. *Chem. Rev.* **1993**, *93* (1), 571–584.

(26) Das, P. Transient Carbocations and Carbanions Generated by Laser Flash Photolysis and Pulse Radiolysis. *Chem. Rev.* **1993**, *93* (1), 119–144.

(27) Pischel, U.; Abraham, W.; Schnabel, W.; Müller, U. The Photogeneration of Aryltropylium Ions: A Potential Photo-Switch for Supramolecular Assemblies Based on Donor–Acceptor Interaction. *Chem. Commun.* **1997**, *15*, 1383–1384.

(28) Abraham, W.; Buck, K.; Orda-Zgadzaj, M.; Schmidt-Schäffer, S.; Grummt, U.-W. Novel Photoswitchable Rotaxanes. *Chem. Commun.* **2007**, *29*, 3094–3096.

(29) Raskosova, A.; Stößer, R.; Abraham, W. Molecular Photo-switches Based on Spiro-Acridans. *Chem. Commun.* **2013**, *49* (38), 3964–3966.

(30) Agmon, N. Mechanism of Hydroxide Mobility. *Chem. Phys. Lett.* **2000**, *319* (3), 247–252.

(31) Marx, D.; Chandra, A.; Tuckerman, M. E. Aqueous Basic Solutions: Hydroxide Solvation, Structural Diffusion, and Comparison to the Hydrated Proton. *Chem. Rev.* **2010**, *110* (4), 2174–2216.

(32) Eom, K.; Yoon, D. S.; Lee, S. W.; Lee, G.; et al. Nanomechanical Actuation Driven by Light-Induced DNA Fuel. *Chem. Commun.* **2012**, *48* (7), 955–957.

(33) Liu, H.; Xu, Y.; Li, F.; Yang, Y.; Wang, W.; Song, Y.; Liu, D. Light-Driven Conformational Switch of i-Motif DNA. *Angew. Chem., Int. Ed.* **2007**, *46* (14), 2515–2517.

(34) Carvalho, C. P.; Uzunova, V. D.; Da Silva, J. P.; Nau, W. M.; Pischel, U. A Photoinduced pH-Jump Applied to Drug Release from Cucurbit[7]uril. *Chem. Commun.* **2011**, *47* (31), 8793–8795.

(35) Zhou, D.; Khatmullin, R.; Walpita, J.; Miller, N. A.; Luk, H. L.; Vyas, S.; Hadad, C. M.; Glusac, K. D. Mechanistic Study of the Photochemical Hydroxide Ion Release from 9-Hydroxy-10-methyl-9-phenyl-9, 10-dihydroacridine. *J. Am. Chem. Soc.* **2012**, *134* (28), 11301–11303.

(36) Xie, Y.; Luk, H. L.; Yang, X.; Glusac, K. D. Excited-State Hydroxide Ion Transfer from a Model Xanthenol Photobase. *J. Phys. Chem. B* **2015**, *119*, 2498–2506.

(37) Prémont-Schwarz, M.; Barak, T.; Pines, D.; Nibbering, E. T.; Pines, E. Ultrafast Excited-State Proton-Transfer Reaction of 1-Naphthol-3, 6-Disulfonate and Several 5-Substituted 1-Naphthol Derivatives. *J. Phys. Chem. B* **2013**, *117* (16), 4594–4603.

(38) Keitz, B. K.; Yu, C. J.; Long, J. R.; Ameloot, R. Lithographic Deposition of Patterned Metal−Organic Framework Coatings Using a Photobase Generator. *Angew. Chem., Int. Ed.* **2014**, *53* (22), 5561–5565.

(39) Cameron, J. F.; Willson, C. G.; Fréchet, J. M. Photogeneration of Amines from α-Keto Carbamates: Photochemical Studies. *J. Am. Chem. Soc.* **1996**, *118* (51), 12925–12937.

(40) Sun, X.; Gao, J. P.; Wang, Z. Y. Bicyclic Guanidinium Tetraphenylborate: A Photobase Generator and a Photocatalyst for Living Anionic Ring-Opening Polymerization and Cross-Linking of Polymeric Materials Containing Ester and Hydroxy Groups. *J. Am. Chem. Soc.* **2008**, *130* (26), 8130–8131.

(41) Peters, M. V.; Stoll, R. S.; Kühn, A.; Hecht, S. Photoswitching of Basicity. *Angew. Chem., Int. Ed.* **2008**, *47* (32), 5968–5972.

(42) He, J.; Kimani, F. W.; Jewett, J. C. A Photobasic Functional Group. *J. Am. Chem. Soc.* **2015**, *137* (31), 9764–9767.

(43) Gleu, K.; Schubert, A. Die Kondensation der Phosphoroxy-chlorid-Acridone mit Dimethylanilin. *Ber. Dtsch. Chem. Ges. B* **1940**, *73* (7), 757–761.

(44) Jones, G.; Farahat, M. S.; Greenfield, S. R.; Gosztola, D. J.; Wasielewski, M. R. Ultrafast Photoinduced Charge-Shift Reactions in Electron Donor-Acceptor 9-Arylacridinium ions. *Chem. Phys. Lett.* **1994**, *229* (1), 40–46.

(45) Deno, N.; Jaruzelski, J.; Schriesheim, A. Carbonium Ions. I. An Acidity Function (C0) Derived from Arylcarbonium Ion Equilibria1. *J. Am. Chem. Soc.* **1955**, *77* (11), 3044–3051.

(46) Ito, S.; Morita, N.; Asao, T. Syntheses of Azulene Analogues of Triphenylmethyl Cation: Extremely Stable Hydrocarbon Carbocations and the First Example of a One-Ring Flip as the Threshold Rotation Mechanism for Molecular Propellers. *Bull. Chem. Soc. Jpn.* **1995**, *68* (5), 1409–1436.

(47) Zhang, X.-M.; Bruno, J. W.; Enyinnaya, E. Hydride Affinities of Arylcarbenium Ions and Iminium Ions in Dimethyl Sulfoxide and Acetonitrile. *J. Org. Chem.* **1998**, *63* (14), 4671–4678.

(48) Pines, D.; Pines, E. *Solvent Assisted Photoacidity*; Wiley-VCH: Weinheim, Germany, 2007; Vol. *1*, p 377.

(49) Hansch, C.; Leo, A.; Taft, R. A Survey of Hammett Substituent Constants and Resonance and Field Parameters. *Chem. Rev.* **1991**, *91* (2), 165–195.

(50) Pines, E.; Fleming, G. R. Proton Transfer in Mixed Water-Organic Solvent Solutions: Correlation between Rate, Equilibrium Constant, and the Proton Free Energy of Transfer. *J. Phys. Chem.* **1991**, *95* (25), 10448–10457.

(51) Tolbert, L. M.; Harvey, L. C.; Lum, R. C. Excited-State Proton Transfer from Hydroxyalkylnaphthols. *J. Phys. Chem.* **1993**, *97* (50), 13335–13340.

(52) Minto, R. E.; Das, P. K. Laser Flash Photolysis Study of Photodehydroxylation Phenomena of 9-Phenylxanthen-9-ol and Photobehavior of Related Intermediates. Enhanced Electrophilicity of 9-Phenylxanthenium Cation Singlet. *J. Am. Chem. Soc.* **1989**, *111* (24), 8858–8866.

(53) Haynes, W. M. *CRC Handbook of Chemistry and Physics*; CRC Press, 2014.

(54) Dalton, J. C.; Montgomery, F. C. Solvent Effects on Thioxanthone Fluorescence. *J. Am. Chem. Soc.* **1974**, *96* (19), 6230–6232.

(55) Cavaleri, J. J.; Prater, K.; Bowman, R. M. An Investigation of the Solvent Dependence on the Ultrafast Intersystem Crossing Kinetics of Xanthone. *Chem. Phys. Lett.* **1996**, *259* (5), 495–502.

(56) Marcus, R. A. On the Theory of Oxidation-Reduction Reactions Involving Electron Transfer. I. *J. Chem. Phys.* **1956**, *24* (5), 966–978.

(57) Marcus, R. On the Theory of Oxidation-Reduction Reactions Involving Electron Transfer. II. Applications to Data on the Rates of Isotopic Exchange Reactions. *J. Chem. Phys.* **1957**, *26* (4), 867–871.

(58) Marcus, R. Chemical and Electrochemical Electron-Transfer Theory. *Annu. Rev. Phys. Chem.* **1964**, *15* (1), 155–196.

(59) Miller, J.; Calcaterra, L.; Closs, G. Intramolecular Long-Distance Electron Transfer in Radical Anions. The Effects of Free Energy and Solvent on the Reaction Rates. *J. Am. Chem. Soc.* **1984**, *106* (10), 3047–3049.

(60) Johnston, H. S.; Parr, C. Activation Energies from Bond Energies. I. Hydrogen Transfer Reactions. *J. Am. Chem. Soc.* **1963**, *85* (17), 2544–2551.

(61) Chandra, A.; Rao, V. S. An Examination of the BEBO Model with the Results of Ab Initio Calculations of a Reaction Series. *Chem. Phys.* **1994**, *187* (3), 297–303.

(62) Marcus, R. A. Theoretical Relations among Rate Constants, Barriers, and Brønsted Slopes of Chemical Reactions. *J. Phys. Chem.* **1968**, *72* (3), 891–899.

(63) Marcus, R. A. On the Theory of Electron-Transfer Reactions. VI. Unified Treatment for Homogeneous and Electrode Reactions. *J. Chem. Phys.* **1965**, *43* (2), 679–701.

(64) Oevering, H.; Paddon-Row, M. N.; Heppener, M.; Oliver, A. M.; Cotsaris, E.; Verhoeven, J. W.; Hush, N. S. Long-Range Photoinduced Through-Bond Electron Transfer and Radiative Recombination via Rigid Nonconjugated Bridges: Distance and Solvent Dependence. *J. Am. Chem. Soc.* **1987**, *109* (11), 3258–3269.

(65) Hupp, J. T.; Weaver, M. J. Noncontinuum Solvent Effects upon the Intrinsic Free-Energy Barrier for Electron-Transfer Reactions. *J. Phys. Chem.* **1985**, *89* (9), 1601–1608.

(66) Chen, P.; Meyer, T. J. Medium Effects on Charge Transfer in Metal Complexes. *Chem. Rev.* **1998**, *98* (4), 1439–1478.

(67) Nelsen, S. F.; Trieber, D. A.; Ismagilov, R. F.; Teki, Y. Solvent Effects on Charge Transfer Bands of Nitrogen-Centered Intervalence Compounds. *J. Am. Chem. Soc.* **2001**, *123* (24), 5684–5694.

(68) Xi, W.; Peng, H.; Aguirre-Soto, A.; Kloxin, C. J.; Stansbury, J. W.; Bowman, C. N. Spatial and Temporal Control of Thiol-Michael Addition via Photocaged Superbase in Photopatterning and Two-Stage Polymer Networks Formation. *Macromolecules* **2014**, *47* (18), 6159–6165.

(69) Zhang, X.; Xi, W.; Wang, C.; Podgórski, M.; Bowman, C. N. Visible-Light-Initiated Thiol-Michael Addition Polymerizations with Coumarin-Based Photobase Generators: Another Photoclick Reaction Strategy. *ACS Macro Lett.* **2016**, *5* (2), 229–233.

(70) Bell, R. P. *The Proton in Chemistry*; Springer Science & Business Media, 2013.

(71) March, J. *Advanced Organic Chemistry: Reactions, Mechanisms, and Structure*; John Wiley & Sons, 1992.